Dosimetry of a D2/D3 Dopamine Receptor Antagonist That Can Be Used with PET or SPECT

P. David Mozley, James B. Stubbs, Hee-Joung Kim, Will McElgin, Sumalee Chumpradit, Mei-Ping Kung, Gemma Romaniello and Hank F. Kung

Division of Nuclear Medicine, University of Pennsylvania Medical Center, Philadelphia, Pennsylvania; and Radiation Internal Dose Information Center, Oak Ridge Institute for Science and Education, Oak Ridge, Tennessee

FIDA-2 {R-(+)-2,3-dimethoxy-5-iodo-N-[(1-4'-fluorobenzyl)-2-pyrrolidinyl) methyl] benzamide} is a simultaneously fluorinated and iodinated D2/D3 dopamine receptor antagonist. The purpose of this study was to measure its biodistribution and radiation dosimetry in humans. **Methods:** Whole-body emission scans were sequentially acquired in eight healthy volunteers 24–43 hr after the intravenous administration of 101–150 MBq ^{123}I FIDA-2. Regions of interest (ROIs) were placed on the initial set of conjugate emission images and transposed as a single set onto all the other scans without manipulating any of the regions for solid organs independently. The counts in each ROI were corrected for attenuation with transmission scans and compared to the net counts in images of the injection syringe containing the administered dose. The radiation doses were estimated with the MIRD formalism from the residence times for both the ^{18}F- and ^{123}I-labeled ligands. **Results:** There were no subjective or objective pharmacological effects of the tracer on any of the subjects. The findings showed that the dose-limiting organ for the ^{123}I-labeled product was the thyroid gland in this sample. If the ^{18}F-labeled product had been used, then the urinary bladder would have received 0.086 mGy/MBq (0.32 rads/mCi) and become the dose-limiting organ. The effective dose equivalents were 0.025 mSv/MBq (0.092 rem/mCi) for both the ^{123}I- and the ^{18}F-labeled versions of the tracer. **Conclusion:** The data suggest that FIDA-2 can be used to produce relatively high contrast images of the D2/D3 dopaminergic system with substantially less than the maximum allowable radiation dose for research volunteers.

Key Words: FIDA-2; dosimetry; dopamine receptor; positron emission tomography; single-photon emission computed tomography

J Nucl Med 1995; 36:1322–1331

There is much evidence to suggest that dopaminergic transmission participates in the mediation of normal cognition, emotion and movement (*1–3*). Dopaminergic dysfunction may contribute to the formation of several neuropsychiatric symptoms (*4–7*). This has led to the development of radiopharmaceuticals that can be used clinically to visualize different components of the dopaminergic system (*8–10*). Several radioligands have been labeled with ^{18}F to study the postsynaptic D2 receptors with PET (*11–14*). Other postsynaptic D2 receptor ligands have been labeled with ^{123}I for use with SPECT (*15–22*). A radiopharmaceutical that could be used with either PET or SPECT without changing its biological properties may have several advantages. Alternatively labeling a radiopharmaceutical with either ^{123}I or ^{18}F will not change its biological properties if the molecule is both fluorinated and iodinated anyway and the radionuclide is simply substituted for the stable form of the isotope at the same position.

FIDA-2 {R-(+)-2,3-dimethoxy-5-iodo-N-[(1-4'-fluorobenzyl)-2-pyrrolidinyl) methyl] benzamide} is a simultaneously fluorinated and iodinated benzamide analog (Fig. 1). Preclinical pharmacology studies have shown that FIDA-2 is a selective D2/D3 dopamine receptor antagonist (*23*). In vitro binding studies in Sf9 cell lines, which selectively overexpress D2 or D3 dopamine receptors, have shown that FIDA-2 has a K_d for the D2 receptor of 0.04 n*M*, and a K_d for the D3 receptor of 0.05 n*M* (*24*). Ex vivo autoradiography has demonstrated that the basal ganglia-to-cerebellar uptake ratio of FIDA-2 at 1 hr postintravenous injection averaged 13.1–1 in anesthetized rats (*23*). Preclinical studies in nonhuman primates have demonstrated preferential uptake in the basal ganglia with a target-to-background contrast ratio of 6.3 ± 2.9 after 1 hr and 8.14 ± 4.7 after 2 hr (*24*). Dynamic SPECT scans in monkeys have shown that both direct- and indirect-acting dopaminergic drugs can affect the uptake and elimination kinetics of FIDA-2 in the basal ganglia. These findings have suggested that FIDA-2 may be a useful imaging agent for studying D2/D3 receptors in humans, which led to this study of its biodistribution and radiation dosimetry in healthy volunteers.

Received Apr. 25, 1994; revision accepted Aug. 8, 1994.
For correspondence or reprints contact: P. David Mozley, MD, 110 Donner Building, H.U.P., 3400 Spruce St., Philadelphia, PA 19104.

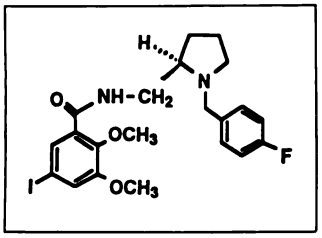

FIGURE 1. The chemical formula for FIDA-2. Substituting ^{18}F for fluorine or ^{123}I for iodide will not change the biological properties of the ligand.

METHODS

Subjects

The protocol was approved by the local Human Subjects Committee (IRB) and the Radioactive Drug Research Committee. The first five men and three women to meet the inclusion criteria and give informed consent participated in the dosimetry phase of the study. The pharmacokinetics of FIDA-2 in the brain were studied in the next two women and another man. The subjects had a mean age of 31.0 ± 7.9 yr (range: 20–41 yr). The men had an average weight of 85 kg (185 lb) and a mean height of 180 cm (5′11″). The women weighed an average of 75 kg (166 lb) and had a mean height of 173 cm (5′8″). All the volunteers were subjectively healthy. Each one was either fully employed (n = 6) or a full-time student. None of them were affiliated with our medical school or its hospital. Only one subject was associated with the university.

Structured medical histories were taken and physical examinations were performed. None of the volunteers had a history of a disease process that could have significantly affected the biodistribution or elimination of the radioligand at the time of study, although one man had a past history of a single hospitalization for pneumonia. None of the subjects were taking any medication at the time of the study other than oral contraceptive pills. They were all pretreated with 9 drops of Lugol's solution containing about 67.5 mg potassium iodide about 90 min before injection.

Blood was drawn and urine was collected for routine laboratory analyses about an hour before tracer administration. Most tests were repeated 24 hr later. The clinical laboratory battery included a complete blood cell count with differential measurements of serum electrolyte concentrations, assays of blood urea nitrogen, creatinine, glucose, cholesterol, triglycerides, total serum protein, uric acid, antinuclear antibody levels, complement levels, liver function tests and thyroid function tests which included TSH levels. Serum cortisol levels were assayed. Follicle stimulating hormone (FSH) and leutinizing hormone (LH) levels were measured in the women. Pregnancy was ruled out by measuring beta-Human chorio-gonadotrophic (β-HCG) levels in the serum.

Radionuclide

The sodium [^{123}I]-iodide used in this study was obtained commercially (Nordion Intl., Kanata, Canada) and was produced with an enriched ^{124}Xe target. The manufacturer guaranteed that the radionuclidic purity of each dose exceeded 99.8% at the time of delivery. The specific activity was 2.4×10^5 Ci/mmole.

Radiolabeling

The preparation of the tributyl tin precursor has already been described in detail (*23*). The radiolabeling process began by adding 50 μl of 1 N hydrochloric acid (HCl) to a shipping vial containing about 12 mCi of sodium (Na) ^{123}I. The acidified solution was transferred to a kit containing 50 μg of lyophilized 5-tributylstannyl-FIDA-2. The iodination reaction was initiated by adding 50 μl of a 3% hydrogen peroxide solution and quenched 20 min later with 100 μl of a saturated sodium bisulfite solution. The solution was then neutralized with sodium bicarbonate and extracted with ethyl acetate three times. The combined extracts were passed through a column containing anhydrous sodium sulfate. The anhydrous ethyl acetate eluent was condensed to dryness under a stream of nitrogen gas. The residue was redissolved in 100 μl ethanol and injected into a high-pressure, liquid chromatography (HPLC) system equipped with a reverse-phase column. The product was eluted with a mobile phase consisting of acetonitrile-pH 7.0 buffer ammonium phosphate (5 m*M*, 90/10). The fraction of the eluant corresponding to ^{123}I-FIDA-2 was separated and collected. Ascorbic acid (100 μg) was added as an antioxidant before the solution was condensed. The residue was then redissolved in 100 μl ethanol and diluted with 3 ml saline. The final solution was passed through a 0.22-μm filter prior to administration.

A small portion of the final product was analyzed for purity by coinjecting it into an HPLC column along with a standard solution of nonradioactive FIDA-2 and the specific activity was determined. Other aliquots were retained for sterility and pyrogenicity tests.

The radiochemical purity of the final product always exceeded 95%. The theoretical specific activity of the no-carrier-added ^{123}I-FIDA-2 was 240,000 Ci/mmole (*23*). The detection limits of the UV spectrometer used in this study limited specific activity measurements to >50,000 Ci/mmole.

Measurements of Administered Activity

The amount of radioactivity in each syringe containing ^{123}I-labeled FIDA-2 was measured in a dose calibrator (Radcal 4045, Monrovia, CA) before and after injection. The mean dose administered during the whole-body distribution phase was 127 ± 16 MBq (3.43 ± 0.43 mCi) with a range of 101–150 MBq (2.73–4.05 mCi). Conjugate images of the doses in their injection syringes were also acquired before and after administration on one of two identical dual-headed cameras equipped with large field of view, low-energy, parrallel-hole collimators (Prism 2000, Picker International, Cleveland, OH). A conjugate set of static images was obtained for 2 min followed by a 10-min scan in the whole-body mode. The acquisition parameters for the syringe images were identical to the ones used to scan the patients and acquire the transmission images.

Transmission Images

A transmission source was prepared by dissolving 150–300 MBq ^{123}I in 1600 ml of water, which was contained in a Lucite sheet flood. Its rectangular dimensions were about the same size as the collimators on the dual-headed scanner. The flood was filled with water several hours before the radioactivity was added. This reduced bubble formation during scanning by allowing the water temperature to approach equilibrium with the ambient room temperature. The water level was topped off after the sodium ^{123}I in it had been mixed by manual shaking. The flood was taped on top of the posterior projection collimator. The distance between the sheet source and the surface of the anterior projection collimator on the upper head was always 42.5 cm.

Nonattenuated scans of the transmission source were obtained in the whole-body mode by acquiring transmission images on the upper camera while the sheet source moved in tandem on the lower head. The scans were acquired for 10 min each over an excursion of 194–205 cm, which corresponded to 98–94 sec/pixel, respectively. The maximum speed for collimator travel was less

than 0.39 to 0.41 cm/sec, which tended to minimize fluid motion within the flood.

The imaging table was then replaced, and the subjects were positioned in the center of the field of view. A whole-body transmission scan was then performed for 20 min. Otherwise, the acquisition parameters were identical to the ones used to acquire the nonattenuated transmission flood images and the subsequent emission scans.

Emission Images

The sequence of measurements was designed to acquire the early emission images immediately after the transmission scans without moving the subject so that the two sets of images would be optimally coregistered. The radiopharmaceutical was injected rapidly as a bolus through an indwelling catheter in an antecubital vein while dynamic images of the thorax and abdomen were acquired for 2 sec per frame for 60 frames. A series of static 256 × 256 images were then acquired for 30 sec per frame for 16 frames without moving the collimators. These images were used to localize organs that did not take up enough activity for visualization on the delayed images. The first whole-body scan was acquired 10 min after injection. Each whole-body scan was acquired in a 256 × 1024 matrix for 20 min over a total excursion length that ranged from 194 to 205 cm. The pixel size was 2.18 mm^2, which corresponded to a scan time of 197–188 sec/pixel, respectively. The first 4–5 whole-body scans were obtained over the next 4–6 hr. Delayed images were obtained the next morning between 13–16 hr after injection and the next evening between 23 and 26 hr after injection. The last two subjects in the sample had additional imaging for 40–43-hr postinjection. The mean number of discreet, nonsuccessive emission scans was 7.25 (range: 6–8) in this sample.

SPECT images of the brain were acquired for 30 min about 2 hr after injection in the first eight subjects. Dynamic SPECT scans of the brain were obtained in the next three subjects for 5 min each for 2 hr after administration. All SPECT images were acquired on a triple-headed camera equipped with high-resolution fanbeam collimators. The images were reconstructed with a count rate-dependent filter. The modulation transfer function (MTF) was generated from the line spread function of the camera (*25*). Chang's method was used to correct for attenuation (*26*). Validation of the image analysis technique used to measure regional brain activity has been previously described (*27*).

Renal Excretion Fractions

Subjects were asked to void frequently during the first evening of study and collect urine samples overnight. A mean of 6.0 (range 4–8) discreet samples were obtained from each subject. Specimens collected in relatively small containers were imaged after transferral into large, plastic bedpans. Specimens collected in 3000-ml plastic bottles were laid out flat on the imaging table. Conjugate images of all the individual urine specimens were acquired with the same parameters used to obtain the static 256 × 256 images of the injection syringes containing the administered dose. Checks were performed by measuring the volume of urine in each specimen and the activity in a 20-ml aliquot in the same dose calibrator used to measure the injection syringes. The camera counts in the urine specimen images, however, were subsequently used for analysis.

Image Analysis

The images were exported into a graphics workstation (Sun Microsystems, Mountain View, CA). The image analysis package limited the display to any 256 × 512 pixels from the original 256 × 1024 pixels in the whole-body scan. This limited the field of view to 56 × 112 cm (22 × 44 inches) and required the air above the head and the distal portions of the lower extremities to be interactively cut out of the display. Since the whole body did not fit in the 256 × 512 display, another independent program was used to automatically measure the total number of counts in the original 256 × 1024 images. Regions of interest (ROIs) were drawn around 14 organs and the whole (256 × 512 pixel) field of view on the earliest set of emission images. The ROIs were then transposed as a single set onto all the other images, including the transmission scans through air and the subject. It was occasionally necessary for an operator to move the entire set of ROIs as a single unit to correct small repositioning errors between scans. It was also necessary to periodically adjust the size of the ROIs for the stomach, gallbladder and urinary bladder to account for normal changes in volume. Changes in the height of the urinary bladder required the inferior border of the ROI representing the whole abdomen to be moved accordingly. Otherwise, the individual ROIs were rarely manipulated independently of the other regions in the set. An automated subroutine measured the number of counts in these ROIs. A representative example is shown in Figure 2 which corresponds to Subject 5 in the tables.

Corrections for Linear Attenuation

The ROIs drawn on the first set of emission images were transposed to both the nonattenuated image of the sheet flood and the transmission scan through the subject as a single unit without operator interaction. An attenuation factor was calculated for each ROI by dividing the number of counts in it on the transmission scan through the subject by the number of counts in it on the nonattenuated transmission image. The counts in the corresponding ROIs on the emission images were subsequently divided by this ratio during geometric mean calculations for each conjugate image set.

Calculating the Activity in an Organ

The total counts in conjugate images of the injection syringes, the urine specimens and the ROIs were exported into a computerized spread sheet where they were corrected for decay and attenuation. Geometric means for each pair of conjugate ROIs were calculated and normalized for unit time. The fraction of the injected dose at each time point was then estimated by dividing the corrected count rates in each ROI by the net count rates in the injection syringes containing the doses. The formula was given by Equation 1 below (*28–31*):

$$C_{i(t)} = \frac{\sqrt{(C_{a.ROI} \times D_{f(t)}) \times (C_{p.ROI} \times D_{f(t)})}}{(C_{t.subj} \div C_{t.air})} \Big/ C_{net.dose}, \qquad \text{Eq. 1}$$

where $C_{i(t)}$ is the fraction of the administered dose in a given ROI at time t; $C_{a.ROI}$ is the anterior view count rate in the ROI at time t (cpm); $C_{p.ROI}$ is the posterior view count rate in the ROI at time t (cpm); $C_{t.air}$ are the counts in the ROI on the nonattenuated images of the flood (cpm); $C_{t.subj}$ are the counts in the ROI on the transmission scan through the subject (cpm); $D_{f(t)}$ is the decay factor for time t, where $Df(t) = \exp[1n(2) \times (t \div 13.2)]$; and $C_{net.dose}$ is the net counts in the conjugate images of the injection syringes (cpm)

$$= \sqrt{(C^{\circ}_{a.dose} \times C^{\circ}_{p.dose})} - \sqrt{(C'_{a.dose} \times D_{f(t_d)})\,(C'_{p.dose} \times D_{f(t_d)})}, \qquad \text{Eq. 2}$$

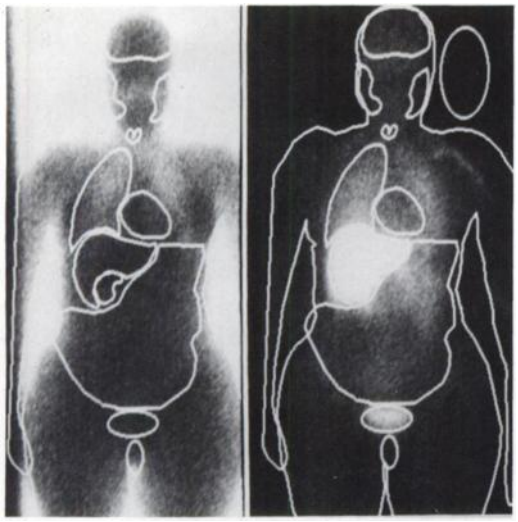

FIGURE 2. Anterior images of Subject 5. The image analysis technique allowed assembly of the ROIs which were on the earliest emission image (B) and then transposed as a single set onto all the other scans, including the transmission scans (A). The relative intense activity in the gallbladder and the urinary bladder on this 12–32-min postinjection image was typical of all the subjects and indicates rapid excretion of FIDA-2 by the renal and enterohepatic systems. The line of activity in the left upper extremity on the emission image was also seen in each subject and probably represents uptake and retention in the brachial vasculature of the injected arm.

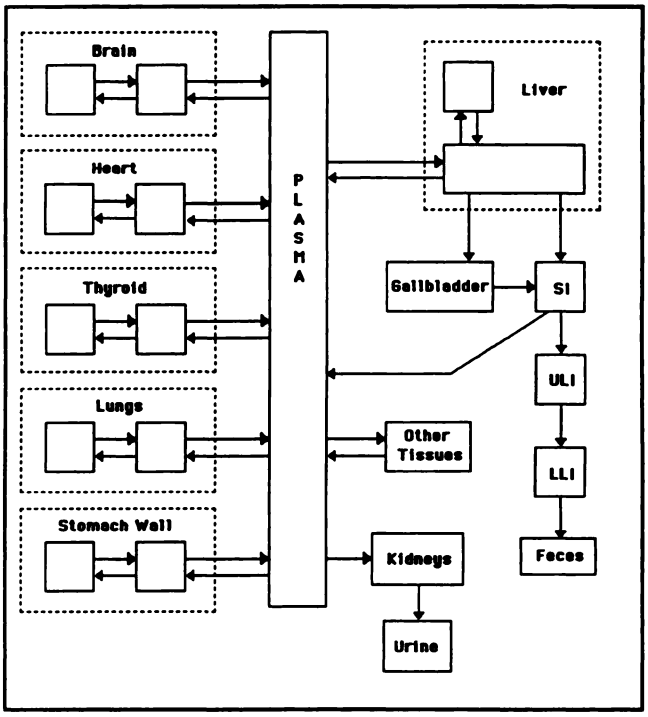

FIGURE 3. Schematic diagram of the multicompartmental model used to describe ^{123}I-labeled FIDA-2 biokinetics.

where C° is the counts in the injection syringe containing the administered dose (cpm); C′ is the residual counts in the injection syringe after administration (cpm); and $D_{f(t_d)}$ is the decay factor for the residual dose left in the injection syringe.

Checks were performed by adding the fraction of the dose in the ROI representing the whole field of view to the fraction of the dose excreted in the urine up until that time, and comparing the sum to the net counts in the injection syringes.

Organ Residence Times

Time-activity curves were generated directly from the experimental data for the brain, gallbladder, genitalia, heart, kidney, liver, right lung, stomach, thyroid and the whole abdominal compartment excluding the liver and the urinary bladder. The time-activity curves for these organs and nine other tissues in the body were fitted with a multicompartmental model developed specifically to estimate organ residence times from the experimental data (Fig. 3). The Simulation Analysis and Modeling (SAAM) software used to mathematically fit the experimental data to the multicompartmental model has been previously described (*31–36*). It did not make any assumptions about the mechanism of FIDA-2 metabolism or its pharmacokinetic behavior other than its tissue distribution and excretion pathways.

The experimental measurements of urine activity were used to model urinary excretion rates. The residence times for the urinary bladder, however, and the dosimetry estimates that followed were based on a theoretical bladder voiding interval of 4.8 hr, or five times a day (*37*).

Activity not excreted in the urine was assumed to be eliminated in the feces. All counts in the ROIs for the stomach were assumed to come from activity within the stomach wall. It was also assumed that 30% of the activity excreted by the liver in the bile filled the gallbladder, while the other 70% flowed directly into the small intestine (*38*). The model assumed that the gallbladder ejected its contents into the duodenum in response to a meal once every 6 hr (*37,38*). Each gallbladder cycle consisted of a filling phase lasting 4 hr followed by a contraction phase of 2 hr. The transfer rate coefficient of 1.8 hr^{-1} from the gallbladder to the small intestine was derived by taking the grand mean of the average emptying rates reported in three other studies (*39,40*). The gallbladder residence times were calculated by integrating the activity retention times predicted by the multicompartmental model. The activity entering the lumen of the bowel was assumed to be transferred through the alimentary canal according to the kinetic model for the gastrointestinal tract in ICRP 30 (*41*). The standard mass of tissue in each region of the gut was taken from ICRP 23 (*42*).

The residence times were used to estimate the absorbed doses with the MIRD technique (*43*) for a standard adult male phantom (*44*). The organ doses were calculated for each subject independently before the results were averaged. The dose estimates for the ^{18}F-labeled version of FIDA-2 were calculated from the time-activity curves for the ^{123}I-labeled product after substituting the appropriate physical parameters for ^{18}F in the model. A unit of activity from the ^{18}F-labeled product was estimated to deliver more of an absorbed dose to the source organs than the ^{123}I version of FIDA-2 because ^{18}F generates nine times the nonpenetrating energy per transfer than ^{123}I (*45*).

Metabolite Analysis

The plasma concentrations of the parent compound and its radioactive metabolites were measured in six subjects. Venous blood samples were aspirated 30, 60, 90 and 120 min after injection and placed in preweighed, heparanized tubes. The net weight of the blood in each specimen was measured before the total amount of radioactivity in the whole blood was measured in a gamma counter (Packard Cobra II, Downers Grove, IL). After counting, the plasma was separated from the formed elements by centrifu-

gation for 2 min at 2000 rpm. The volume of plasma was measured and 100 μg of nonradioactive FIDA-2 were added from a standard stock of known concentration and purity. The plasma was then extracted three times with an equal volume of ethyl acetate. The ethyl acetate layers were combined before counting. The aqueous layer was counted separately to determine the percentage of activity in the organic and nonorganic layers. The ethyl acetate was then dried under a stream of nitrogen gas. The residue was dissolved in 100 μl EtOH and injected into a high-performance liquid chromatograph (HPLC) equipped with a reverse-phase column. The activity was eluted at a flow rate of 1 ml/min with an isocratic solvent (90% acetonitril (CH3CN) and 10% 5 m*M* 3,3'-dimethylglutarate (DMGA), pH 7.0). Chemical analysis with an online UV spectrometer was used to identify the fraction containing the parent compond and verify its elution with the standard. Fractions were collected at 1-min intervals for a total of 20 min. The radioactivity in each fraction was counted and corrected for activity loss during processing by applying a previously measured recovery coefficient. The recovery coefficient for each subject was measured separately by the addition of a known quantity of ^{123}I-FIDA to a sample of blood aspirated before injection and processed with identical centrifugation, extraction and chromatographic analysis procedures as the postinjection samples.

RESULTS

There were no subjective effects of the radiotracer on any of the healthy volunteers. Their vital signs remained stable throughout the procedure, and there were no changes noted on physical examination nor were there meaningful changes in any of the clinical laboratory assays performed 24 hr after tracer administration.

Images of the administered doses contained a mean ± s.d. count rate of 684,000 ± 69,000 cpm (range: 512,000–755,000). Concommitantly performed calibration studies showed that this count rate was well within the linear response range of both cameras. Retrospectively pooling the data from both cameras showed that the correlation coefficient r describing the relationship between the eight measured doses and the corresponding camera counts was 0.989.

The nonattenuated transmission source images contained a mean of 3.40 million counts (range, 2.16–4.45 million). Grid analysis of the actual data over the useful field of view showed that the count rates in 1000 pixel boxes had an internal s.d. that was always less than 10%. The variance between different regions of the field was always less than 10%. The transmission scans through the subjects, which were acquired for twice as long as the nonattenuated images, contained similar numbers of counts in the whole field of view. The sum of the attenuation-corrected counts in the 256 × 512 emission images plus the activity already voided in the urine never deviated by more than 5% from the total number of transmission corrected counts in the initial set of emission images. During the first 16 hr of the study, the total activity that could be accounted for never varied by more than 2.5% in four subjects and was less than 1.5% in two subjects. The average dose recovered in each individual subject ranged from 94% to 104% of the injected activity (mean = 97%).

The images show that FIDA-2 was excreted by both the enteroheopatic and the renal systems. Activity could be visualized in the urinary bladder on the first whole-body emission image in every subject. In seven subjects, the experimentally measured renal excretion fractions ranged from 23.4% to 29.7% during the first 16 hr with a mean of 26%. One subject failed to collect any urine overnight. Four urine specimens were obtained from this subject, however, during the first 5 hr of the study. The model predicted that his total renal excretion fraction over an infinitely long time period would have been 25.4%. This is very close to the mean value of 25.5% ± 1.7% predicted by the model for the other seven subjects (range 21.1%–28.1%).

The hepatic uptake was rapid and peaked on the first set of emission images. The effective residence times were longest in the liver for both ^{123}I- and ^{18}F-FIDA-2 of the tracer. The time-activity curve for the gallbladder resembled an inverted "U" in most subjects. The model predicted that the mean fecal excretion fraction was 21.4% ± 4.2% (range 14.8%–24.2%).

The maximum decay-corrected activity in the ROI for the thyroid gland always occurred on the first emission image and ranged from 0.262% to 0.074% of the injected dose with a mean of 1.53%. The fraction of the dose in the ROI for the thyroid gland decreased with each successive measurement in six subjects. It increased between the 16- and 24-hr measurements in the other two volunteers by 0.024% and 0.028% of the injected dose.

Analysis of the plasma showed that the fraction of activity associated with polar metabolites, which included free ^{123}I, increased with time from an average of 19.6% at 30 min postinjection to 46% at 120 min postinjection. The findings showed that the fraction of activity in the plasma associated with the intact parent compound decreased with time from 85% ± 10% after 30 min to 64% ± 10% after 120 min (Fig. 4). HPLC showed that there was at least one nonpolar metabolite in the ethyl acetate layer besides the parent compound. The metabolite was eluted faster than FIDA-2 from the reverse-phase column. The metabolite peak could be observed on the 30-min plasma sample from every subject. The fraction of activity associated with this metabolite peak increased with time in each subject.

The dynamic SPECT data showed that uptake in the dopaminergic regions of the brain peaked at 20–40 min postinjection. The planar images showed that the mean activity fraction in the brain at 20 min postinjection was 2.65% ± 0.56% (range: 1.75%–4.11%). Time-activity curves for the brain are shown in Figure 5. Profiles for regions of specific binding in the brain were relatively flat between 30 and 120 min of injection (Fig. 5A). The rate of elimination from the basal ganglia was slower than the washout rate from regions of nonspecific binding in the rest of the brain. The caudate-to-occipital cortex contrast ratio at 2 hr postinjection ranged from 5.6 to 11.0 (Fig. 6).

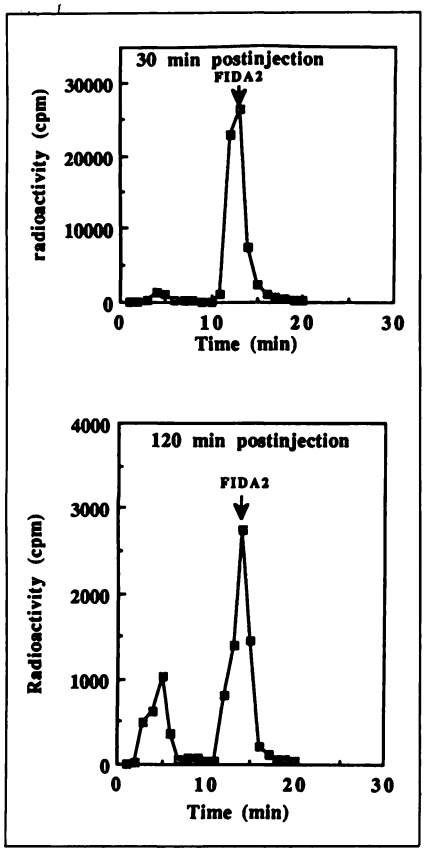

FIGURE 4. HPLC metabolite profiles. Analysis showed that 85% and 64% of the extractable activity was still bound to the parent FIDA-2 molecule after 30 and 120 min, respectively.

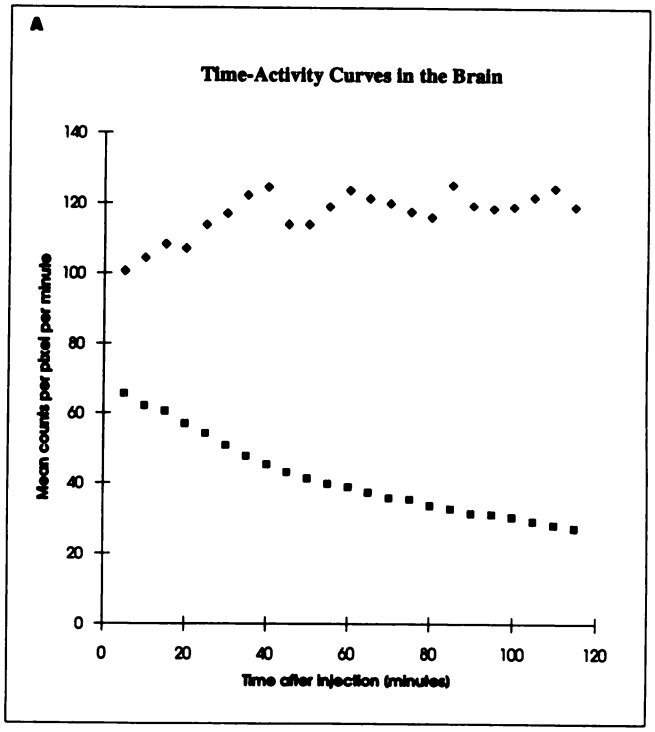

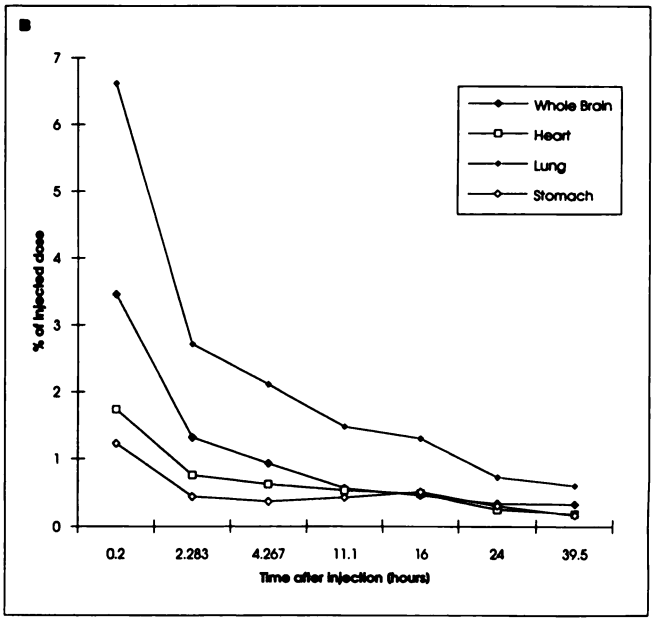

FIGURE 5. (A) Time-activity curves for the caudate and whole brain show that the rate of elimination from regions of specific binding is slower than the washout from the rest of the brain. (B) Time-activity curves for several organs, including the brain. The findings show that elimination of FIDA-2 from most organs is relatively rapid.

Table 1 lists the effective organ residence times for ^{123}I- and ^{18}F-FIDA-2 in all eight subjects individually.

Table 2 lists the absorbed dose estimates for ^{123}I-FIDA-2 in this study. The 67.5 mg potassium iodide administered before injection did not completely prevent visualization of activity in the thyroid on the delayed images. The thyroid appeared to be the dose-limiting organ for ^{123}I-FIDA-2. The organs of excretion received the next largest doses of radiation. If the uptake of free iodide had been more completely blocked, the dose-limiting organ for ^{123}I-FIDA-2 would have been the distal colon. It absorbed 0.062 ± 0.085 mGy/MBq (0.23 rad/mCi). The radiation burden to the proximal colon was almost as high at 0.056 ± 0.079 mGy/MBq, followed by the doses to the urinary bladder wall (0.45 ± 0.034 mGy/MBq) and the gallbladder (0.038 ± 0.047 mGy/MBq). The effective dose equivalent (EDE) was 0.025 mSv/MBq (0.092 rem/mCi).

The biodistribution of ^{18}F-FIDA-2 was assumed to be identical to the biodistribution of the ^{123}I-FIDA-2. The calculations, however, showed that the effective residence times for the ^{18}F-FIDA-2 were different because the physical half-life of the PET tracer is much shorter than the physical half-life of ^{123}I. Since the physical half-life of ^{18}F is also much shorter than the biological half-life of FIDA-2 in most tissues, the relative dose decreased to organs with relatively slow uptake and/or protracted biological retention, such as the colon. Conversely, the relative dose increased in organs with relatively rapid uptake and clearance, such as the heart, lungs and gallbladder. The results of the dosimetry calculations for ^{18}F-FIDA-2 are listed in Table 3. The dose-limiting organ for ^{18}F-FIDA-2 was the urinary bladder wall, which received 0.086 mGy/MBq (0.32 rads/mCi). The effective dose equivalent (EDE) for ^{18}F-

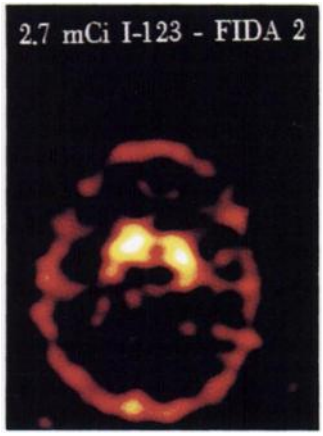

FIGURE 6. Transaxial image of a healthy human brain at the level of the diencephalon. The images were acquired with only 100 MBq (2.7 mCi) ^{123}I-FIDA-2 on a triple-headed SPECT system equipped with fanbeam collimators. A count rate dependent prefilter was applied before the images were corrected for attenuation.

labeled FIDA-2 was the same as the EDE for ^{123}I-FIDA-2 at 0.025 mSv/MBq (0.092 rem/mCi).

DISCUSSION

The findings show that relatively high resolution images of the postsynaptic D2/D3 dopamine receptor can be produced with FIDA-2 in humans. The dosimetry estimates for both ^{18}F- and ^{123}I- FIDA-2 appear favorable. Administering up to 500 MBq (15 mCi) of either tracer will conform to federal safety guidelines for research volunteers. FIDA-2 also appears to be a pharmacologically safe radioligand. The 40–400-pmole quantities that were administered did not cause any side effects in this group of healthy volunteers.

The true margin of safety may be even higher. The dose-limiting organ for the PET version of FIDA was the urinary bladder. This estimate was based, however, on a theoretical interval of 4.8 hr between the time of injection and the elimination of any activity from the bladder. In clinical practice, the absorbed dose to the urinary bladder wall can probably be reduced substantially by encouraging subjects to micturate right after the neuroimaging procedure.

The dose-limiting organ for the ^{123}I-labeled tracer appeared to be the thyroid. Although some of the counts in the ROI for the thyroid may have actually come from the intact parent compound or its organic metabolites, most of the activity was probably attributable to the uptake of free ^{123}I. The study subjects were pretreated with a single 67.5-mg dose of potassium iodide. This is only half of the dose recommended to achieve thyroid blockage of 95%–

TABLE 1
Residence Times for Iodine-123-I-FIDA-2 and Fluorine-18-F-FIDA-2 (hr)

	Subjects							
Organ	1	2	3	4	5	6	7	8
^{123}I-FIDA-2								
Liver	0.71	1.2	1.4	1.2	0.74	1.3	1.2	0.85
Colon (ULI)	0.49	0.073	0.94	1.1	0.60	1.1	0.91	0.84
Colon (LLI)	0.38	0.58	0.75	0.86	0.48	0.89	0.72	0.68
Lung	0.57	0.61	0.88	0.65	0.59	0.61	0.91	0.52
Bladder	0.52	0.46	0.44	0.42	0.49	0.43	0.44	0.47
Bowel, small	0.25	0.37	0.48	0.55	0.30	0.57	0.46	0.43
Brain	0.10	0.17	0.21	0.13	0.11	0.098	0.13	0.14
Gallbladder	0.050	0.10	0.13	0.14	0.08	0.15	0.12	0.12
Heart	0.130	0.29	0.27	0.17	0.12	0.18	0.11	0.090
Stomach	0.090	0.15	0.70	0.56	0.21	0.09	0.047	0.080
Kidney	0.040	0.040	0.040	0.038	0.040	0.040	0.041	0.040
Thyroid	0.070	0.017	0.22	0.12	0.060	0.12	0.070	0.040
Remainder of body	3.9	3.5	2.	3.2	3.8	3.3	3.4	3.6
^{18}F-FIDA-2								
Liver	0.11	0.25	0.30	0.32	0.18	0.33	0.26	0.24
Lungs	0.12	0.15	0.19	0.17	0.14	0.15	0.31	0.18
Bladder	0.17	0.15	0.15	0.14	0.16	0.14	0.14	0.15
Bowel, small	0.034	0.072	0.092	0.099	0.058	0.11	0.084	0.081
Colon (ULI)	0.018	0.040	0.050	0.055	0.032	0.060	0.046	0.045
Brain	0.034	0.040	0.070	0.041	0.036	0.003	0.038	0.043
Gallbladder	0.013	0.032	0.040	0.043	0.026	0.050	0.036	0.036
Heart	0.038	0.050	0.050	0.035	0.036	0.036	0.031	0.029
Kidney	0.023	0.020	0.020	0.018	0.021	0.019	0.018	0.020
Stomach	0.022	0.020	0.11	0.086	0.034	0.011	0.011	0.019
Colon (LLI)	0.003	0.007	0.009	0.001	0.006	0.010	0.008	0.008
Thyroid	0.007	0.003	0.019	0.010	0.006	0.009	0.006	0.004
Remainder of body	1.4	1.3	1.0	1.2	1.4	1.2	1.2	1.3

ULI = upper large intestine; LLI = lower large intestine.

TABLE 2
Radiation Dosimetry Estimates for Iodine-123-FIDA-2

Target organ	Mean (mGy/MBq)	Mean (rad/mCi)	Minimum (mGy/MBq)	Maximum (mGy/MBq)	% s.d.
Thyroid*	9.70E-02	3.60E-01	2.10E-02	2.30E-01	68%
Bowel, lower large intestine†	6.20E-02	2.30E-01	3.80E-02	8.10E-02	24%
Bowel, upper large intestine†	5.60E-02	2.10E-01	3.40E-02	7.30E-02	25%
Urinary bladder‡	4.50E-02	1.70E-01	4.20E-02	4.90E-02	5%
Gallbladder wall*	3.80E-02	1.40E-01	2.00E-02	4.90E-02	26%
Stomach*	3.10E-02	1.10E-01	6.00E-03	9.00E-02	103%
Liver§	2.60E-02	9.70E-02	1.80E-02	3.30E-02	23%
Small bowel†	2.40E-02	8.90E-02	1.60E-02	3.10E-02	21%
Lungs*	2.00E-02	7.50E-02	1.60E-02	2.60E-02	19%
Heart wall*	1.90E-02	6.90E-02	1.20E-02	2.80E-02	34%
Ovaries§	1.50E-02	5.60E-02	1.10E-02	1.90E-02	17%
Uterus§	1.20E-02	4.30E-02	1.00E-02	1.30E-02	9%
Pancreas§	9.10E-03	3.40E-02	7.20E-03	1.20E-02	20%
Kidneys‡	9.00E-03	3.30E-02	7.90E-03	9.90E-03	8%
Bone surfaces§	8.50E-03	3.10E-02	8.20E-03	8.70E-03	2%
Adrenals§	7.70E-03	2.90E-02	6.80E-03	8.70E-03	9%
Spleen§	6.10E-03	2.30E-02	5.40E-03	7.50E-03	14%
Bone marrow, red§	5.80E-03	2.20E-02	5.30E-03	6.20E-03	5%
Muscle§	5.30E-03	2.00E-02	5.00E-03	5.60E-03	4%
Thymus§	5.10E-03	1.90E-02	4.60E-03	5.50E-03	5%
Brain*	4.80E-03	1.80E-02	3.70E-03	6.60E-03	21%
Testes§	4.20E-03	1.60E-02	3.70E-03	4.50E-03	6%
Breasts§	3.70E-03	1.40E-02	3.50E-03	3.90E-03	4%
Skin§	2.90E-03	1.10E-02	2.70E-03	3.00E-03	3%
Eyes, lens§	5.50E-04	2.00E-03	1.10E-04	1.60E-03	103%
Effective dose equivalent	2.5E-02 [mSv/MBq]	9.2E-02 [rem/mCi]	1.8E-02 [mSv/MBq]	3.2E-02 [mSv/MBq]	21%

*Estimated from experimentally placed ROIs.
†Estimated from a single ROI for the abdomen.
‡Estimated from conjugate images of voided urine specimens.
§Estimated from the model.

98% (*46*). In clinical practice, the uptake of free ^{123}I can probably be reduced with higher dosing regimens of potassium iodide.

The variability in the dose estimates for most organs was relatively small. This could reflect the application of narrow inclusion crtieria to a small population. It may also represent, however, the enhanced precision obtained with a dual-headed scanner that simultaneously acquires conjugate views of the whole body. The conjugate images were always optimally opposed in space and time. The whole-body views prevented large ROIs, such as the one representing the entire abdomen, from being broken across the images. The image analysis technique allowed a single set of ROIs to be placed on each scan without operator manipulation. Even after the activity became too low to visualize the exact boundary of an organ on the delayed images, the original ROI could still be replaced by making sure the other regions, such as the head and whole body, fit well. The image analysis technique also tended to increase the accuracy of attenuation correction. Some of the potential problems that could have been produced by nonuniformity in the field of view were minimized by placing the ROI for an organ in the same position on the nonattenuated flood and subject transmission scans.

Subtle repositioning errors occurred on some of the later emission scans. Most of the errors, however, were simple translations in the axial direction that could be corrected by moving the entire set of ROIs as a single unit. The attenuation and scatter in hollow organs such as the stomach and gallbladder varied over the course of the study with normal circadian changes in volume. The dose estimates to the bladder were not affected, however, because they were based on measurements of voided activity.

CONCLUSION

These findings indicate that both ^{18}F- and ^{123}I-labeled FIDA-2 may be relatively safe and potentially effective tracers for imaging D2/D3 dopamine receptors in humans.

TABLE 3
Radiation Dosimetry Estimates for Fluorine-18-FIDA-2

Target organ	Mean (mGy/MBq)	Mean (rad/mCi)	Minimum (mGy/MBq)	Maximum (mGy/MBq)	% s.d.
Urinary bladder*	8.60E-02	3.20E-01	7.80E-02	9.90E-02	8%
Thyroid†	7.00E-02	2.60E-01	2.90E-02	1.60E-01	58%
Gallbladder wall†	6.90E-02	2.60E-01	3.10E-02	9.70E-02	29%
Stomach†	4.00E-02	1.50E-01	1.10E-02	1.10E-01	95%
Liver†	3.70E-02	1.40E-01	1.90E-02	4.80E-02	26%
Lungs†	3.60E-02	1.30E-01	2.60E-02	5.90E-02	28%
Heart wall†	3.00E-02	1.10E-01	2.40E-02	3.70E-02	15%
Bowel, upper large intestine wall‡	2.80E-02	1.10E-01	1.60E-02	3.60E-02	23%
Small bowel‡	2.60E-02	9.40E-02	1.60E-02	3.30E-02	21%
Kidneys*	2.00E-02	7.30E-02	1.90E-02	2.00E-02	2%
Uterus§	1.50E-02	5.50E-02	1.40E-02	1.50E-02	4%
Bowel, lower large intestine wall‡	1.40E-02	5.30E-02	1.20E-02	1.60E-02	10%
Adrenals§	1.30E-02	4.60E-02	1.10E-02	1.30E-02	6%
Ovaries§	1.30E-02	4.70E-02	1.20E-02	1.40E-02	5%
Pancreas§	1.30E-02	4.90E-02	1.20E-02	1.50E-02	8%
Bone marrow§	1.00E-02	3.80E-02	9.70E-03	1.10E-02	4%
Spleen§	1.00E-02	3.70E-02	9.50E-03	1.10E-02	5%
Thymus§	9.40E-03	3.50E-02	8.80E-03	9.90E-03	4%
Brain†	8.90E-03	3.30E-02	7.00E-03	1.40E-02	24%
Bone surfaces§	8.70E-03	3.20E-02	8.00E-03	9.30E-03	4%
Muscle§	8.70E-03	3.20E-02	8.10E-03	9.10E-03	3%
Testes§	8.20E-03	3.10E-02	7.20E-03	9.50E-03	9%
Breasts§	7.60E-03	2.80E-02	7.10E-03	8.10E-03	4%
Skin§	6.20E-03	2.30E-02	5.60E-03	6.80E-03	6%
Eye, lens	5.50E-04	7.00E-03	1.50E-04	1.50E-04	96%
Effective dose equivalent	2.5E-02 [mSv/MBq]	9.2E-02 [rem/mCi]	1.8E-02 [mSv/MBq]	3.2E-02 [mSv/MBq]	21%

*Estimated from conjugate images of voided urine specimens
†Estimated from experimentally placed ROIs
‡Estimated from a single ROI for the abdomen
§Estimated from the model

ACKNOWLEDGMENTS

This study was partially supported by National Institutes of Health grant NS-24538 and National Institute of Mental Health grant MH-43880. The work at Oak Ridge was performed under Interagency Agreement No. FDA 224-75-3016, DOE 40-286-71. Oak Ridge Associated Universities performs complementary work for the U.S. Department of Energy under contract DE-AC05-76OR00033.

REFERENCES

1. Seeman P. Brain dopamine receptors. *Pharmacol Rev* 1980;32:229–269.
2. Alexander GE, Crutcher MD, DeLong MR. Basal ganglia-thalamocortical circuits: parallel substrates for motor, oculomotor, "prefrontal" and "limbic" function. In: Uylings HBM, Van Edin CG, De Bruin JPC, Corner MA, Feenstra MGP, eds. *Progress in brain research*, volume 85; New York: Elsevier Science Publishers; 1990:119–146.
3. Stoof J, Kebabian J. Two dopamine receptors: biochemistry, physiology, and pharmacology. *Life Sci* 1984;35:2281–2296.
4. Peroutka SJ, Snyder SH. Relationships of neuroleptic drug effects at brain dopamine, serotonin, a-adrenergic, and histamine receptors to clinical potency. *Am J Psychiatry* 1980;137:518–522.
5. Carlsson A. The current status of the dopamine hypothesis in schizophrenia. *Neuropsychopharmacol* 1988;1:179–186.
6. Goeders NE, Kuhar MJ. Chronic cocaine administration induced opposite changes in dopamine receptors in the striatum and nucleus accumbens. *Science* 1983;221:773–775.
7. Dewey SL, Logan J, Wolf AP, et al. Amphetamine induced decreases in (^{18}F)-N-methylspiroperidol binding in the baboon brain using positron emission tomography (PET). *Synapse* 1991;7:324–327.
8. Mazjere B, Coenen HH, Haldin C, Nagren K, Pike VW. PET radioligands for dopamine receptors and re-uptake sites: chemistry and biochemistry. *Nucl Med Biol* 1992;19:497–512.
9. Volkow ND, Fowler JS, Wolf AP, et al. Distribution and kinetics of carbon-11-cocaine in the human body measured with PET. *J Nucl Med* 1992;33: 521–525.
10. Innis RB, Seibyl JP, Scanley BE, et al. Single photon emission computed tomography imaging demonstrates loss of striatal dopamine transporters in Parkinsons disease. *Proc Natl Acad Sci USA* 1993;90:11965–11969.
11. Wagner HN, Burns HD, Dannals RJ. Imaging dopamine receptors in the human brain by positron tomography. *Science* 1983;221:1264–1266.
12. Farde L, Weisel FA, Hall H, Haldin C, Stone-Elauder S, Sedvall G. No D2 dopamine receptor increase in PET study of schizophrenia. *Arch Gen Psychiatry* 1987;44:671–672.
13. Waddington J. Sight and insight: brain dopamine receptor occupancy by neuroleptics visualised in living schizophrenic patients by positron emission tomography. *Br J Psychiat* 1989;154:433–436.
14. Baron JC, Martinot JL, Cambon H, et al. Striatal dopamine receptor occupancy during and following withdrawal from neuroleptic treatment: correlative evaluation by positron emission tomography and plasma prolactin levels. *Psychopharmacol* 1989;99:463–472.
15. Kung HF, Pan S, Kung M-P, et al. In vitro and in vivo evaluation of [^{123}I]IBZM: a potential CNS D-2 dopamine receptor imaging agent. *J Nucl Med* 1989;30:88–92.
16. Hall H, Kohler C, Gawell L. Some in vitro receptor binding properties of [^{3}H] eticlopride, a novel substituted benzamide, selective for the dopamine D2 receptors in the rat brain. *Eur J Pharm* 1985;111:191–199.
17. Murphy RA, Kung HF, Kung M-P, Billings JJ. Synthesis and characteriza-

tion of iodobenzamide analogs: potential D-2 dopamine receptor imaging agents. *J Med Chem* 1990;3:171–178.
18. Janowsky A, de Paulis T, Clanton JA, Smith HE, Ebert MH, Kessler RM. [^{125}I]iodopride: a specific high affinity radioligand for labeling striatal dopamine D2 receptors. *Eur J Pharm* 1988;150:203–205.
19. Kessler RM, Ansari S, de Paulis T, et al. High affinity dopamine D2 receptor radioligands. I. Regional rat brain distribution of iodinated benzamides. *J Nucl Med* 1991;32:1593–1600.
20. Kessler R, Ansari M, Schmidt D, et al. High affinity dopamine D2 receptor radioligands. II. [^{125}I]epidepride, a potent and specific radioligand for the characterization of striatal and extrastriatal dopamine D2 receptors. *Life Sci* 1991;49:617–628.
21. Kung M-P, Kung HF, Billings JJ, Yang Y, Murphy RA, Alavi A. The characterization of IBF as a new selective dopamine D2 receptor imaging agent. *J Nucl Med* 1990;31:648–654.
22. Tatsch K, Schwartz J, Oertel WH, Kirsch CM. SPECT imaging of dopamine D2 receptors with ^{123}I-IBZM in Parkinsonian syndromes. *J Nucl Med* 1991;32:1014–1015.
23. Chumpradit S, Kung M-P, Billings JJ, Mach R, Kung HK. Fluorinated and iodinated dopamine agents: D2 imaging agents for PET and SPECT. *J Med Chem* 1993;36:221–228.
24. Vessotskie J, Kung M-P, Romaniello G, et al. In vivo and in vitro characterization of R(+)-FIDA-2: a novel D2/D3 dopamine receptor imaging agent [Abstract]. *J Nucl Med* 1994;35:128.
25. Kim H-J, Karp JS, Kung HF, Mozley PD. Quantitative effects of a count rate dependent Wiener filter on image quality: a basal ganglia phantom study simulating [I-123] dynamic SPECT imaging [Abstract]. *J Nucl Med* 1993; 34:190.
26. Chang LT. A method for attenuation correction in radionuclide computed tomography. *IEEE Trans Nucl Sci* 1978;25:638–643.
27. Resnick SM, Karp JS, Turetsky BI, Gur RE. Comparison of anatomically-defined versus physiologically based regional localization: effects on PET-FDG quantitation. *J Nucl Med* 1993;34:2201–2207.
28. Budinger TF. Progress in atomic medicine. In: Lawrence JA, ed. *Recent advances in nuclear medicine*, volume 4. New York: Grune and Stratton; 1974:41.
29. Jones JP, Brill AB, Johnson RE. The validity of an equivalent point source assumption used in quantitative scanning. *Phys Med Biol* 1975;20:455–464.
30. Thomas SR, Maxon HR. In vivo quantitation of lesion radioactivity using external counting methods. *Med Phys* 1976;3:253–255.
31. Robertson J. *Compartmental distribution of radiotracers*. New York: CRC Press; 1983:73–142.
32. Stubbs JB, Smith GT, Stabin MG, Eckerman KF, Turner JE. An approach to cellular level dosimetry using compartmental model analysis and dynamic PET. *Proceedings of the Fifth International Symposium on Radiopharmaceutical Dosimetry*. Watson EE, Schlafke-Stelson A, ed.; May 1991:385–395.
33. Stabin M, Taylor A Jr, Eshima D, Wooter W. Radiation dosimetry for technetium-99m-MAG3, technetium-99m-DTPA and iodine-131-OIH based on human biodistribution studies. *J Nucl Med* 1992;33:33–40.
34. Mozley PD, Stubbs JS, Kung HF, Selickson MH, Stabin MG, Alavi A. Biodistribution and dosimetry of ^{123}I IBF: a potent radioligand for imaging the D2 dopamine receptor. *J Nuc Med* 1993;34:1910–1917.
35. Dey HM, Seibyl JP, Stubbs JB, et al. Human biodistribution and dosimetry of the SPECT benzodiazepine receptor radioligand [I-123]iomazenil. *J Nucl Med* 1994;35:399–404.
36. van Dyck CH, Seibyl JP, Stubbs JB, et al. Human biodistribution and dosimetry of the SPECT D2 receptor radioligand [^{123}I]IBF. *Nucl Med Biol*; in press.
37. Cloutier RJ, Smith SA, Watson EE, Snyder WS, Warner GG. Dose to the fetus from radionuclides in the bladder. *Health Phys* 1973;25:147–161.
38. Molino G, Hofmann A, Cravetto C. Simulation of the metabolism and enterohepatic circulation of endogenous chenodeoxycholic acid in man using a pharmacokinetic model. *Eur J Clin Invest* 1986;16:397–414.
39. Lawson M, Everson G, Klingensmith W, Kern F Jr. Coordination of gastric and gallbladder emptying after ingestion of a regular meal. *Gastroenterology* 1983;85:866–870.
40. Bobba V, Krishnamurthy G, Kingston E, et al. Gallbladder dynamics induced by a fatty meal in normal subjects and patients with gallstones: concise communication. *J Nucl Med* 1984;25:21–24.
41. International Commission on Radiation Protection. Limits for intake of radionuclides by workers. *ICRP Publication 30*. Pergamon Press: New York; 1979.
42. ICRP. Task group report on reference man. *ICRP Publication 23*. Oxford: Pergamon Press; 1975.
43. Loevinger R, Berman M. A revised schema for calculating the absorbed dose from biologically distributed radionuclides. *MIRD pamphlet no. 1*, revised. New York: Society of Nuclear Medicine; 1975.
44. Cristy M, Eckerman K. Specific absorbed fractions of energy at various ages from internal photon sources. *ORNL/TM-8381*. Oak Ridge, TN: Oak Ridge National Laboratory; 1987.
45. Weber DA, Eckerman K, Dillman LT, Ryman J. *MIRD radionuclide data and decay schemes*. New York: Society of Nuclear Medicine; 1989.
46. National Council on Radiation Protection and Measurement (NRCP). Protection of the thyroid gland in the event of releases of radioiodine. *NCRP Report No. 55*; August 1, 1977.